https://doi.org/10.5194/esurf-2022-58
Preprint. Discussion started: 16 November 2022

Earth Surface Dynamics Discussions
Open Access
EGU

Estimating surface water availability in high mountain rock slopes using a numerical energy balance model

Matan Ben-Asher[1], Florence Magnin[1], Sebastian Westermann[2], Emmanuel Malet[1], Johan Berthet[3], Josué Bock[1], Ludovic Ravanel[1], Philip Deline[1].

[1]EDYTEM laboratory, Université Savoie Mont Blanc, CNRS, Le Bourget-du-Lac, 73376, France.
[2]Department of Geosciences, University of Oslo, Oslo, Norway.
[3]Styx 4D, Le Bourget du Lac, France.

Correspondence to: Matan Ben-Asher (matan.ben-asher@univ-smb.fr)

Abstract

Water takes part in most physical processes that shape the mountainous periglacial landscapes and initiation of mass wasting. An observed increase in rockfall activity in several mountainous regions was previously linked to permafrost degradation in high mountains, and water that infiltrates into rock fractures is one of the likely drivers of these processes. However, there is very little knowledge on the quantity and timing of water availability for infiltration in steep rock slopes. This knowledge gap originates from the complex meteorological, hydrological and thermal processes that control snowmelt, and also the challenging access and data acquisition in the extreme alpine environments. Here we use field measurement and numerical modeling to simulate the energy balance and hydrological fluxes in a steep high elevation permafrost affected rock slope at Aiguille du Midi (3842 m a.s.l), in the Mont-Blanc massif. Our results provide new information about water balance at the surface of steep rock slopes. Model results suggest that only ~25% of the snowfall accumulates in our study site, the remaining ~75% are redistributed by wind and gravity. Snow accumulation depth is inversely correlated with surface slopes between 40° to 70°. Snowmelt occurs between spring and late summer and most of it does not reach the rock surface due to the formation of an impermeable ice layer at the base of the snowpack. The annual effective snowmelt, that is available for infiltration, is highly variable and ranges over a factor of six with values between 0.05-0.28 m in the years 1959-2021. The onset of the effective snowmelt occurs between May and August, and ends before October. It precedes the first rainfall by one month on average. Sublimation is the main process of snowpack mass loss in our study site. Model simulations at varying elevations show that effective snowmelt is the main source of water for infiltration above 3600 m a.s.l.; below, direct rainfall is the dominant source. The change from snowmelt-dominated to rainfall-dominated water availability is nonlinear and characterized by a rapid increase in water availability for infiltration. We suggest that this elevation of water availability transition is highly sensitive to climate change, if snowmelt-dominated permafrost-affected slopes experience an abrupt increase in water input that can initiate rock slope failure.

https://doi.org/10.5194/esurf-2022-58
Preprint. Discussion started: 16 November 2022


Earth Surface Dynamics Discussions
Open Access
EGU

1 Introduction

1.1. Water in high mountain periglacial rock slopes

Water plays a key role in the initiation of mass wasting in mountainous periglacial landscapes (French, 2017). Surface water that infiltrates into fractures can transport heat by advection and lead to deep permafrost degradation with a thicker and earlier development of the active layer as compared to pure heat conduction (Hasler et al., 2011; Magnin and Josnin, 2021; Gruber and Haeberli, 2007). Water infiltration is also responsible for mechanical weakening of the rock (Krautblatter et al., 2013) and ice-bonded discontinuities (Haeberli et al., 2010). In large fractures, moving water can create thawing corridors extending deep into permafrost (Hasler et al., 2011). Percolation of water into the tunnels of the Aiguille du Midi (French Alps) cable-car station, noticed every hot summer since the summer heatwave of 2003, is likely caused by this effect (Gruber and Haeberli, 2007). Accumulation of water in deep fractures can potentially result in a hydrostatic head high enough to exert sufficient pressure to initiate failure (Fischer et al., 2010). Water is also an important driver of near surface weathering processes such as frost cracking (Hallet et al., 1991; Hales and Roering, 2007) and acceleration of subcritical cracking over geological time scales (Eppes and Keanini, 2017). However, despite the existing knowledge and ongoing research on water-related mechanical processes in mountainous periglacial landscapes, little knowledge exists on the quantity and timing of water available for infiltration in these environments. This knowledge is becoming increasingly needed with the fast warming of high mountain regions, permafrost warming (Haeberli and Gruber, 2009), and the growing evidence for related increase in rockfall occurrence (Gruber et al., 2004; Allen et al., 2009; Ravanel and Deline, 2011; Huggel et al., 2012; Ravanel and Deline, 2013; Ravanel et al., 2017) as thawing corridors can contribute to the destabilization of large rock volumes, much more than expected in a purely conductive system (*e.g.* Draebing et al., 2014).

This study is aimed to decipher surface moisture availability in steep mountain landscapes and to evaluate its role in surface processes and permafrost degradation processes. To do so, we use a numerical energy balance model coupled with a state-of-the-art snowpack scheme, forced by field measurements, to simulate the processes mentioned above and quantify the flux of excess water that is available for infiltration.

1.2. Estimating snow accumulation and snowmelt on steep slopes

Precipitation in high mountains is composed mostly of snowfall (*e.g.* Naseer et al., 2019). We thus expect snow to be the main source of water in high mountains. A significant portion of the snow that falls on steep slopes does not accumulate due to redistribution by wind and transport by gravity (Sokratov and Sato, 2001; Mott et al., 2010). Previous studies suggested that snow accumulation on steep rock slopes is inversely proportional to the slope angle and that above a certain slope angle, snow does not accumulate (Sommer et al., 2015; Blöschl et al., 1991; Winstral et al., 2002; Gruber Schmid and Sardemann, 2003; Haberkorn et al., 2015). Existing estimations of the threshold angle for snow accumulation range between 45°-80°. This wide

https://doi.org/10.5194/esurf-2022-58
Preprint. Discussion started: 16 November 2022


Earth Surface Dynamics Discussions Open Access EGU

range is likely due to differences in local climatic and topographic conditions in different study areas (Phillips et al., 2017), and perhaps also the resolution of the topographic data used in the analysis (Blöschl et al., 1991; Haberkorn et al., 2017). In this study, we use a site-specific analysis of snow depth distribution from a repeated high-resolution survey of our study site using drone-based photogrammetry. This information is essential to estimate the snow water equivalent amount at the rock slope surface. However, estimations of the water equivalent snowmelt are not enough to evaluate infiltration potential since the actual flux that is available for infiltration is controlled by the hydrological properties of the snowpack and the rock itself. Snowmelt that percolates to the base of the snowpack can refreeze to form an impermeable basal ice layer at the interface between the snow cover and the rock surface, when the rock surface is cold enough to dissipate the latent heat of freezing (Woo and Heron, 1981; Woo et al., 1982; Marsh, 2005) (Supp fig. S1). This ice crust phenomenon was described by Phillips et al. (2016) in an alpine permafrost-affected rock ridge, where they used borehole temperature (T) data to demonstrate how a basal ice layer prevents infiltration of spring snowmelt. To differentiate from the total snowmelt, we use the term 'effective snowmelt' referring to excess water that exceed the field capacity of the snow and occur when the base of the snowpack is permeable and enables infiltration to the rock surface (*i.e.*, when no ice crust exists).

2 Study area

The Aiguille du Midi (AdM) (3842 m a.s.l.; 45.88◦ N, 6.89◦ E) is located on the north-west side of the Mont-Blanc massif (Fig. 1). Its summit consists of three steep peaks (North, Central, and South). The north and west faces tower more than 1000 m above the Glacier des Pélerins and Glacier des Bossons, while the south face is only 250 m high above the Glacier du Géant (Magnin et al., 2015b). The bedrock is composed of porphyritic granite characterized by a N 40◦ E fault network intersected by a secondary network (Leloup et al., 2005). A tourist cable car runs from Chamonix to the AdM peak, where galleries and an elevator are carved in the rock mass and provide year-round access to an extreme and otherwise inaccessible environment. The study site used for the main analysis is located in a ~500 m^2 rock slope on the SE (azimuth angle 150°) face of the central pillar with an average slope of 55°. The study site is equipped with a borehole for T measurements to a depth of 10 m since December 2009 fitted with 10 m length Stump thermistor chains, each with 15 nodes (YSI 44031 sensors, accuracy ±0.1◦C). There are also repetitive high-resolution 3D photogrammetric survey, a time lapse camera and snow depth measurement poles.

https://doi.org/10.5194/esurf-2022-58
Preprint. Discussion started: 16 November 2022

Earth Surface Dynamics Discussions
Open Access
EGU

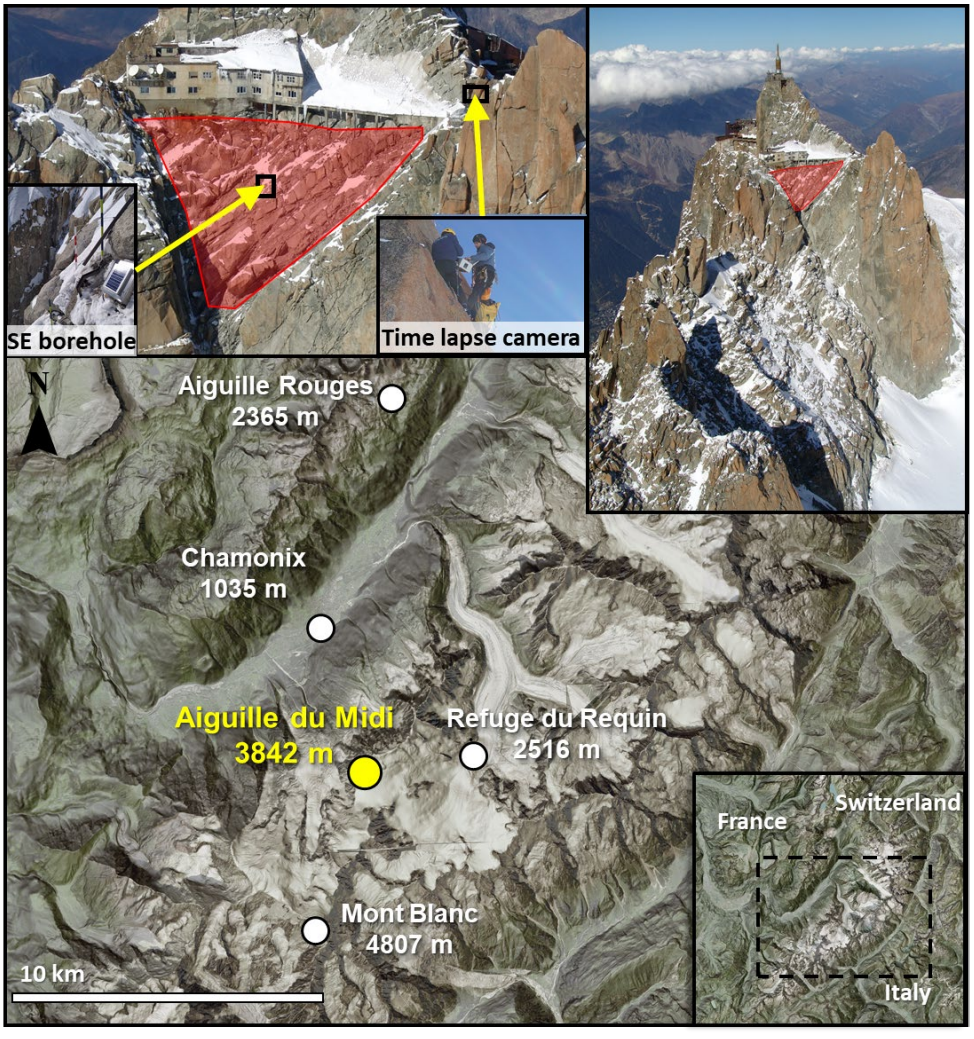

Figure 1: Location map of the study sites and inset map of the Mont-Blanc massif. Top images show the study site on the SE face of Aiguille du Midi (AdM). Red polygon shows the slope area surveyed for high resolution topography using a drone. The small image shows the snow accumulation poles and the borehole on the left, and a time lapse camera installed on the SE pillar on the right, with yellow arrows pointing to their location on the rock slope. Maps provided by the Federal Office of Topography swisstopo.

3 Methods

3.1. Snow depth – spatial distribution

To analyze the spatial distribution of snow depth in our study site, we produced two 3D photogrammetric point cloud models of an area of ~500 m^2 on the SE slope rock surface: one with minimal snow cover, in October 2021, and another with substantial snow cover following heavy snowfall in January 2022 (Fig. 2A-B). Based on our knowledge of the site (first fieldwork in 2005), we assume that the January 2022 snow cover represents conditions close to maximal accumulation. The point clouds

https://doi.org/10.5194/esurf-2022-58
Preprint. Discussion started: 16 November 2022

Earth Surface Dynamics Discussions
Open Access
EGU

were compared by interpolating the elevation data into a 0.1 m cell size digital elevation model (DEM). We calculated local slope and vertical snow depth for each grid pixel (Fig. 2 C-D). The slope was calculated by fitting a second order polynomial surface to a window size of 3×3 pixels and deriving the local gradient (Zevenbergen and Thorne, 1987; Evans, 1980). The main purpose of this analysis was to examine the relation between snow depth and local slope, and also to compare with data from our time lapse camera (see 3.2) to determine the maximum snow depth. We compared the 0.1 m slope-depth relation (Fig. 2C-D) with an upscaled 1 m resolution grid (Fig. 2E-F), which is the length scale of our model realizations, and found the results to be in good agreement.

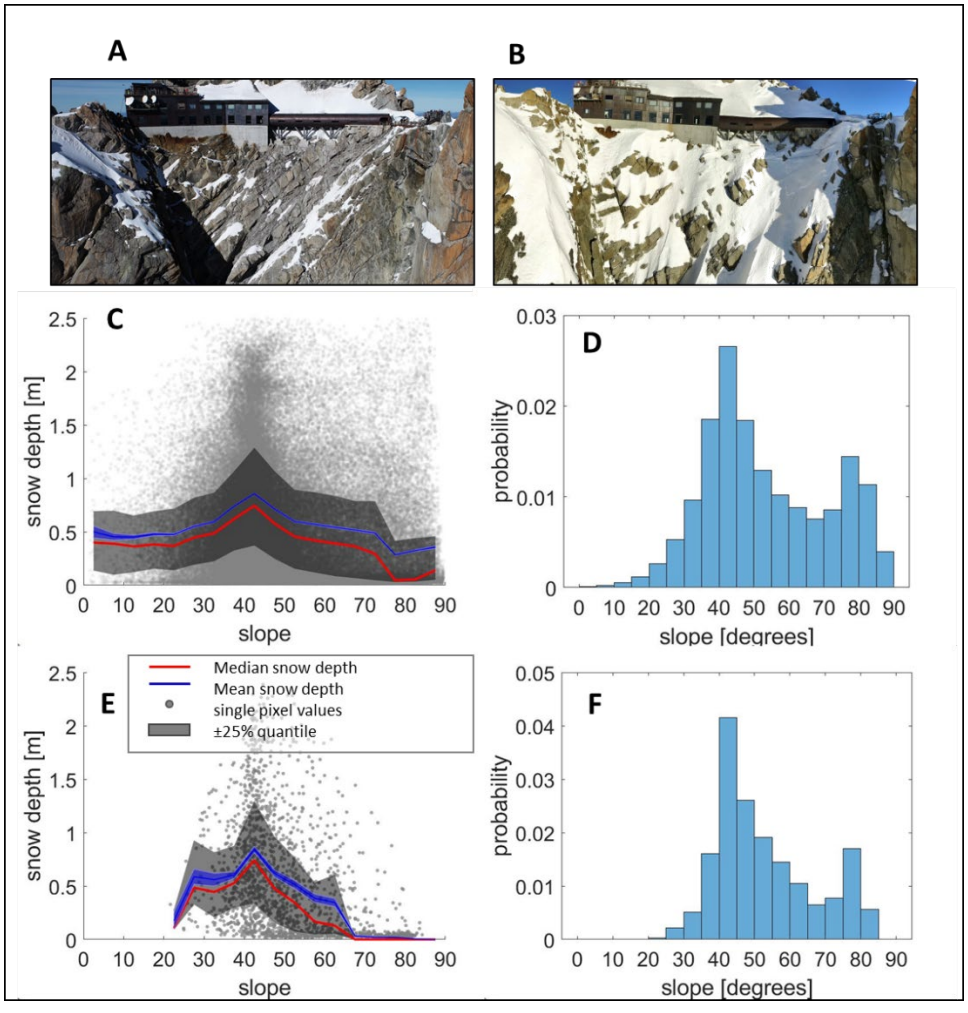

Figure 2: Snow accumulation on steep rock walls - Snow depth vs. local slope from comparison of two 3D photogrammetric point cloud models of an area of 500 m2 on the SE slope rock surface. A) SE face of AdM with minimal snow cover in October 2021. B) SE face of AdM with substantial snow cover in January 2022. C) Snow depth as a function of local slope of the 0.1 m pixels in a high-resolution DEM. Red line is the median value of snow depth for bins of specific local slope (bin size=5°) with ±25% quantile range in gray. Blue line is the mean value with a range of ± standard error. D) Distribution of local slope values. Vertical axis is probability. E-F) Same as C-D after resampling the point cloud data to 1 m cell size. Note that snow depth systematically decreases from median depth of 70 cm at a slope of 40° (and average depth of 80 cm) to <10 cm at 70° slope.

https://doi.org/10.5194/esurf-2022-58
Preprint. Discussion started: 16 November 2022

3.2. Snow depth – temporal distribution

We used time lapse cameras with temporal resolution of several images per day to monitor the height of accumulated snow using permanent measurement poles installed in our study site in AdM (Fig. 1, 4B). We installed 5 poles in an area of 20 m × 20 m near the borehole on the SE face. We used also data that was collected in the same method in 2012 on the E face, near the E borehole. Each pole is 1.4 m high and painted with colored scales of 0.2 m. We produced a snow accumulation time series by visually examining the images with an estimated accuracy of ~5 cm. The snow depth time-series from our field site were then used to calibrate the model constrains on snow accumulation and loss rates, and determine the maximum snow depth. In addition, we used available snow depth measurement from *in-situ* meteorological stations in the Mont-Blanc massif and its area at the Refuge du Requin (https://www.fondation-eng.org/station-meteo) (2516 m a.s.l.) and Aiguilles Rouges – Nivose (*Météo-France* data) (2365 m a.s.l.) (Fig. 1) to compare with the temporal variations in our model results. We assume that the timing of snowfall and accumulation shows a similar trend at the AdM, although the topography and elevation are different and likely to affect the maximum depth. For this reason, we normalized the snow depth at Refuge du Requin and Aiguilles Rouges to the maximum snow depth used in the model run: 80 cm.

3.3. Borehole rock temperature profile

Three boreholes were drilled in 2009 and equipped with T sensors to a depth of ~10 m in 2010 (Magnin et al., 2015b). T sensors depths in the SE borehole are: 0.3, 0.5, 0.7, 0.9, 1.1, 1.4, 1.7, 2.0, 2.5, 3.0, 4.0, 5.0, 7.0, 9.0, 10.0 [m], and in E borehole are: 0.14, 0.34, 0.74, 1.04, 1.34, 1.64, 2.14, 2.64, 3.64, 4.64, 6.64, 8.64, 9.64 [m]. The average T in each depth is stored at time steps of 3 hours. The time *vs* depth measurements of rock T were used to validate the numerical energy balance model.

3.4. Modeling surface energy balance

3.4.1. Model setup

CryoGrid is a toolbox for numerical simulations of ground thermal regime and water balance. Its modular structure makes it suitable for a wide range of terrestrial cryosphere settings and is mainly applied in permafrost environments (Westermann et al., 2022). Previous studies successfully used former CryoGrid models to simulate processes in steep rock walls and mountainous regions (Magnin et al., 2017; Myhra et al., 2017; Schmidt et al., 2021; Legay et al., 2021). We used the CryoGrid community model (version 1.0) toolbox (Westermann et al., 2022) to simulate the 1D ground thermal regime and ice/water balance, and estimate the availability of surface water and its potential for infiltration in rock fractures. In addition to surface energy balance, the CryoGrid model is implemented with the state-of-the-art CROCUS snow scheme (Vionnet et al., 2012) which provides representations of snow cover dynamics, and water drainage. The CROCUS scheme allows for transient representation of internal snow properties as well as interaction processes with the atmosphere and rock (supp. Fig. S2). To

https://doi.org/10.5194/esurf-2022-58
Preprint. Discussion started: 16 November 2022

model water balance at the rock surface, we consider two potential sources of water for infiltration into rock fractures: rainfall and snowmelt. Excess water was set to be produced during snowmelt and rainfall in scenarios when snow water content exceeds its saturated field capacity, if snow cover exists. Snow hydrology is simulated as vertical flow driven by gravity.

3.4.2. Forcing Data

Obtaining reliable and continuous long-term meteorological data from high mountain regions is challenging due to the extreme conditions that limit accessibility and damage equipment. Thanks to the accessibility of the AdM site, meteorological data is available from *in-situ* meteorological stations, including a permanent station of *Météo France* running since 2007. However, the available meteorological data sets contain large gaps and are of limited most duration. We thus compared the available measurements with data obtained from the S2M-SAFRAN meteorological reanalysis tool and found it well fitted for our needs (supp. Fig. S3). The S2M-SAFRAN dataset combines output from a numerical weather prediction model and *in situ* observations, and was originally developed for operational needs to estimate avalanche hazard in mountainous areas (Durand et al., 1993). The S2M-SAFRAN dataset is available for various mountain areas, at elevation steps of 300 m, and with an hourly resolution between the years 1958 to 2021 (Vernay et al., 2022). It includes most parameters that are required for modeling with CryoGrid: Relative humidity, air T, incoming long wavelength radiation, incoming short wavelength solar radiation, and wind speed. To complete the forcing data we used top of the atmosphere incident solar radiation from ERA5 global reanalysis dataset (Hersbach et al., 2020).

3.4.3. Calibration and validation

Our approach to calibrate the model was to fix most parameters with known physical parameters of the study site from the literature (Table 1) (Legay et al., 2021; Magnin et al., 2017) and calibrate the model using two parameters that have predominant impact on snow accumulation: snowfall multiplication factor, and maximum snow depth. The snowfall multiplication factor is a constant value between 0-1 that sets the fraction of snowfall, provided by the meteorological dataset, that can accumulate on the surface. For example, a snowfall fraction value of 0.25 means that only 25% of the net snow fall is accumulated. Maximum snow depth is the maximal depth above which no snow can accumulate once it is reached. The value of maximum snow depth was obtained by comparing two 3D high resolution models of the study site in snow free conditions and after heavy snowfall (see sect. 3.1). For calibration, we used two model outputs that impact snowmelt and that we have field data to compare them with: snow depth and near surface T. We made model runs while iterating over a range of snowfall fraction values and maximum snow depth, and looked for the optimized R^2 and RMSE values of the correlation between observed and modeled near surface T (Fig. 3B). Following the calibration procedure, we validated the model by modeling the T at the E face of AdM using the calibrated model parameters from these faces. The location of the E face borehole shares many characteristics with the SE face borehole (*i.e.* elevation, slope, rock type, meteorology). We compared the near-surface

https://doi.org/10.5194/esurf-2022-58
Preprint. Discussion started: 16 November 2022

Earth Surface Dynamics Discussions
Open Access
EGU

T measured at the E face with the modeled one (Fig. 3C). A north facing borehole also exist at AdM but its location in a vertical wall, above a ledge that locally accumulates snow, makes it impractical for our model settings.

Table 1: Model parameters

Parameter	Value	Units	Source	Remarks
volumetric heat capacity mineral	2×10^{6}	J/m^3K	1	
thermal conductivity	3.3×10^{-3}	W/K	1	
sky view factor	0.63		Calculated using QGIS	
snow fraction	0.25		Calibrated	
heat flux at lower boundary	-0.25	W/m^2	2	
surface albedo	0.16		2	
surface emissivity	0.92		3	
roughness length	0.01	m	2	
maximum snow depth	0.8	m	Field measurement	For slope angle 45°

[1]Legay et al. (2021)
[2]Magnin et al. (2017)
[3]Mineo and Pappalardo (2021)

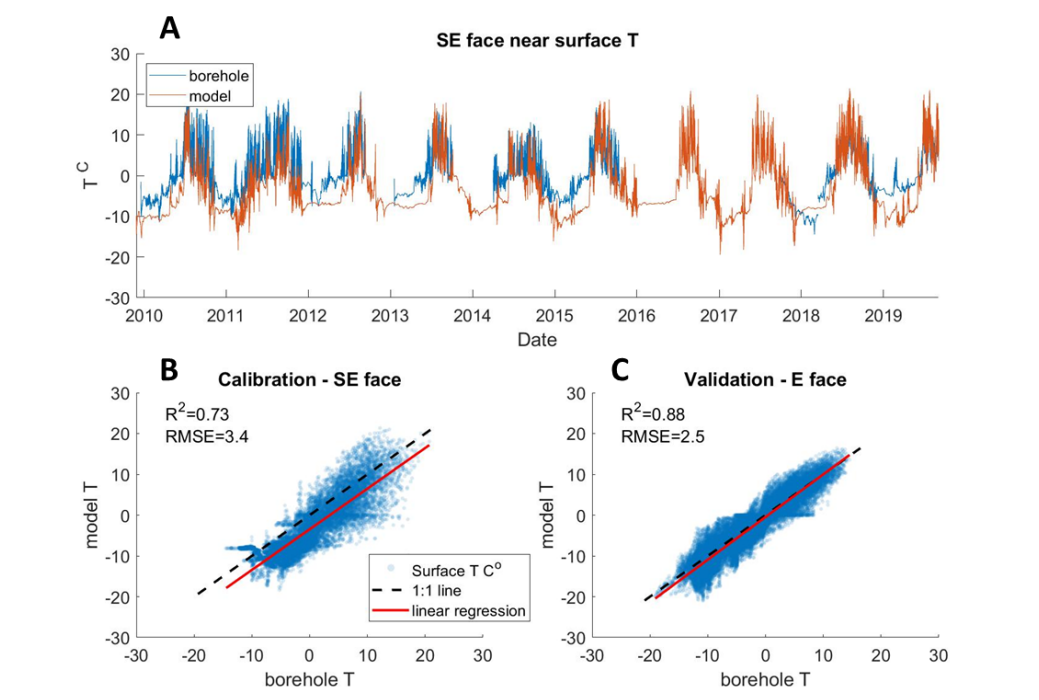

Figure 3: Comparison of near surface T data from model and borehole measurements - A) Comparison of modeled near-surface T (orange) at depth 0.3 m, with borehole measurement from the SE face study site (blue). B) Modeled near surface temperature (depth=0.3 m) as a function of borehole temperature, SE face, after calibration of snow fraction factor (0.25) and maximum snow depth (0.8 m). C) Validating the modeled near surface T at depth 0.14 m, with near-surface T data from a second borehole on the E face of AdM.

https://doi.org/10.5194/esurf-2022-58
Preprint. Discussion started: 16 November 2022


Earth Surface Dynamics Discussions
Open Access
EGU

3.5. Effective snowmelt

Snow density is commonly used as a proxy for snow permeability (Marsh, 2005). We defined a threshold density value at the base of the snowpack for which no infiltration occurs and an ice crust develops (*i.e.*, hydraulic conductivity = 0). Based on an empirical relation suggested by Sommerfeld and Rocchio (1993), we define a threshold density value of 0.4 g/cm^3 which corresponds to a permeability value in range of 10^{-10} m^2 range. In comparison, the average dry snow density in our simulation is 0.24 g/cm^3 with a standard deviation of 0.08 g/cm^3. We thus define effective snowmelt as the volume of water that exceeds the snow pores field capacity during model time steps at which the dry snow density at the base of the snowpack, at the rock-snow contact, is no greater than 0.4 g/cm^3. The CryoGrid model accounts for the inputs of rainfall to the snowpack water balance. To estimate the total potential of water availability for infiltration, we combine the effective snowmelt with the amount of rainfall that falls during partial or no snow cover.

4 Results

4.1. Calibrated model of the SE face of AdM

The optimization process for maximal snow depth and snow multiplication factor in the SE study site resulted in values of 0.8 m and 0.25 respectively. The optimized maximum snow depth value that we found corresponds to what we observed in our snow depth time series from the time lapse camera (see 3.2) and high-resolution snow depth survey (see 3.1). We found that the model results with the S2M-SAFRAN forcing dataset provide satisfying results when comparing the temporal variation of snow accumulation with field measurement from nearby sites at Aiguilles Rouges (R^2=0.52) and Refuge du Requin (R^2=0.49) (Fig. 4A). Modeled rock surface T shows good correlation with borehole data from the SE face of AdM (R^2=0.73) (Fig. 3B). The validation of the model by simulating an E facing slope and comparing with a second borehole located there confirmed that the model is flexible for use within the AdM region and is not single site specific (R^2=0.88) (Fig. 3C).

https://doi.org/10.5194/esurf-2022-58
Preprint. Discussion started: 16 November 2022

Earth Surface Dynamics Discussions
Open Access
EGU

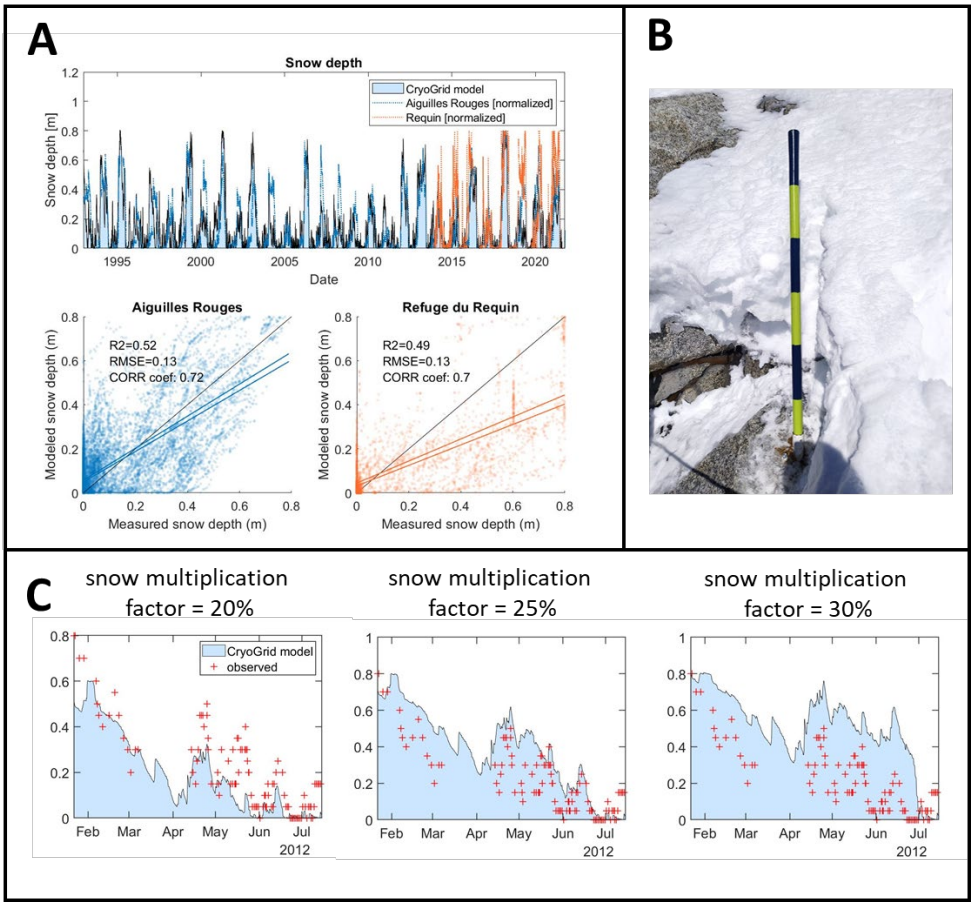

Figure 4: Comparison of modeled snow accumulation with field measurements - A) Comparison of modeled snow depth (black line + light blue area) with snow depth measurement in proximal stations (see Fig. 1 for locations) in the Mont-Blanc massif and its area: Aiguilles Rouges (blue) and Refuge du Requin (orange). Measurements were normalized to 0-0.8 m depth range for comparison. B) Snow depth pole installed on the SE facing rock slope to monitor snow depth time series with a time lapse camera. C) Comparing modeled snow depth, under different snow fraction values used in calibration, with measurements made in-situ using snow poles and time lapse camera. Note the optimum results with snow fraction value of 0.25 (25% accumulation).

4.2. Snow accumulation on steep rock walls

In the calibration process, we found that only about 25% of the snowfall accumulates on the steep rock slopes of our study site on the SE face of AdM. The remaining 75% are likely redistributed by wind and gravity through avalanche and spindrift (*e.g.* Hood and Hayashi, 2010). We found that, for the E face, a snow fraction value of 10% improves the model results, suggesting that conditions are more prone to redistribution of the snowfall. This could be related to the fact the E face is on average 10º steeper than the SE face (average 55º *vs*. 65º).

Topographic analysis of the 10-cm-resolution survey of our field site shows a heterogenous surface with local slope ranging between 20°-90° and a bimodal distribution with two well defined modes at 43° and 80° (Fig. 2D) which illustrate the typical

https://doi.org/10.5194/esurf-2022-58
Preprint. Discussion started: 16 November 2022

steep step-like morphology of the SE rock slope. We resampled the topographic data to 1-m-resolution which is the realization dimension of our numerical model. We found that snow depth systematically decreases from median depth of 70 cm at a slope of 40° (and average depth of 80 cm) to <10 cm at 70° slope. We thus use the value of 80 cm as the maximum value of snow depth in our simulations. At lower slopes, between 25º- 40º, snow depth measurements counter intuitively show a positive correlation. Wirz et al. (2011) reported a similar trend in low slope angles and suggested that it is related to the relatively small area represented. In our case, cells with slope <40° cover ~22% of the surface and cells with slope <30º cover ~ only 6%. Many of the cells with slope <40° are located at a step edge where the snow pack is not supported down slope and accumulation is relatively thin.

4.3. Snowmelt and water availability for infiltration

Figure 5 shows the SE face model results for annual amounts of total snowmelt, effective snowmelt (when the rock surface is penetrable and no ice crust exists at the snowpack bottom), direct rainfall (that falls during times of no or partial snow cover), and sublimation in the SE face of AdM. Most of the annual water mass loss from the snowpack is the result of sublimation (Fig. 5A), especially since sublimation is the only process of snowpack mass loss from November to April at our study site (Fig. 6). Average annual amount of net snowmelt is 0.13 m with a variability that ranges over a factor of six between 0.05-0.28 m, and is directly related to the annual amount of snow accumulation – years with relatively heavy snowfall will get more total snowmelt (Fig. 5B). The annual effective snowmelt ranges between low values of 0.014 m (during the years 1968, 1990, 1992) and highest values of 0.11-0.12 m (during the years 1973, 1975, 1996, 2014). The fraction of effective snowmelt from the total annual excess water (effective snowmelt + runoff + direct rainfall) varies widely from 7 to 90% (during years 1968 and 1975 respectively).

https://doi.org/10.5194/esurf-2022-58
Preprint. Discussion started: 16 November 2022

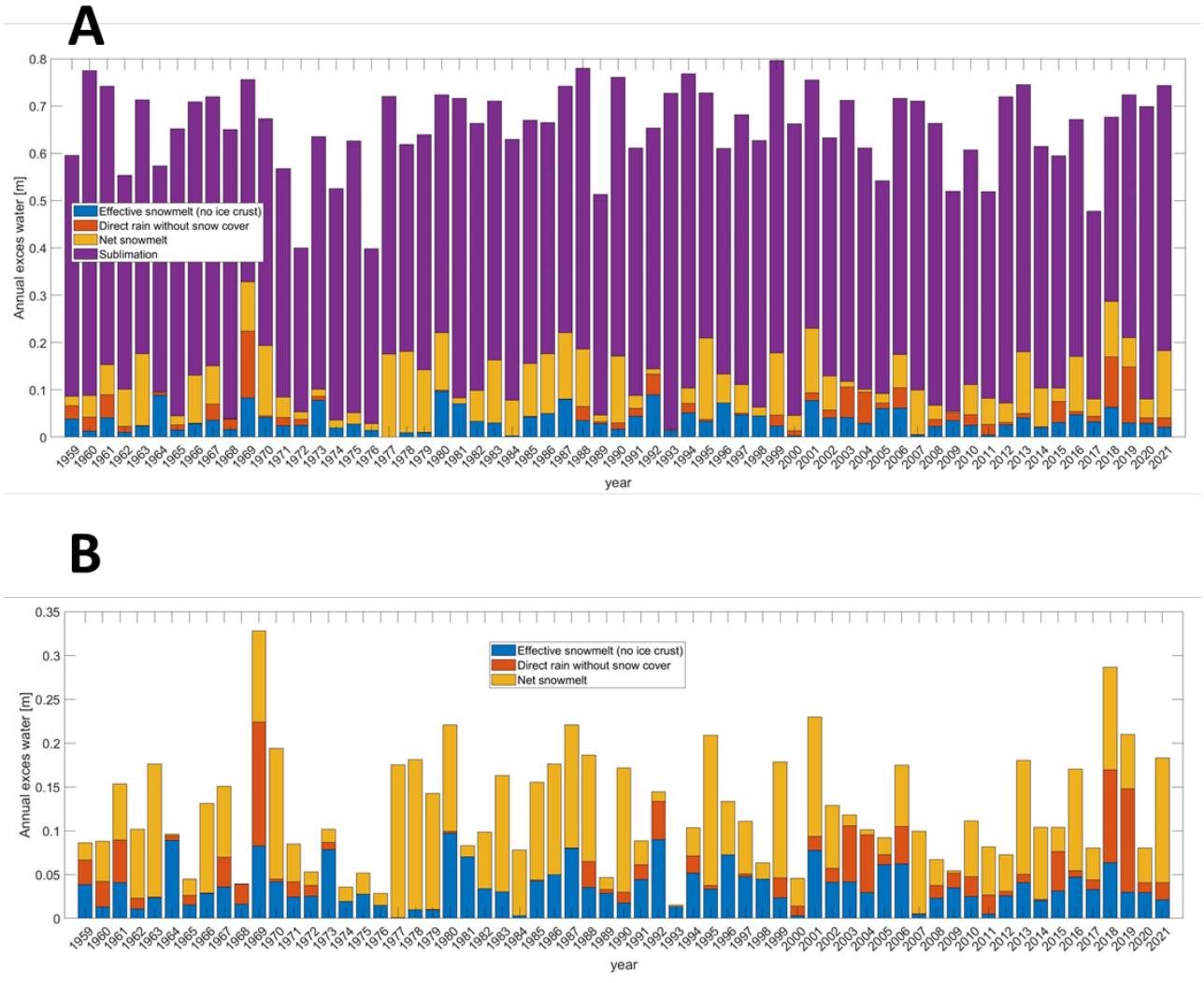

Figure 5: Annual water fluxes in the SE face study site between 1959-2020 - Model results of annual effective snowmelt (blue), direct rain (red), total snowmelt (yellow) and sublimation (purple) in the SE face study site at 3800 m a.s.l. A) Water balance including sublimation. B) Total and effective snowmelt and direct rainfall. Note the high variability in annual water availability for infiltration (effective snowmelt + direct rain), and the high rate of sublimation (bottom image).

On average, in our study site on the SE face, 95% of the snowmelt occur from May to September; however, the effective snowmelt is delayed to the summer months (June to September) when on average 95% of the effective snowmelt occurs (Fig. 6). In most years, effective snowmelt begins in June or July. Few exceptional years show considerable effective snowmelt values in May (1974, 1992, 1996, 2017) and some show first effective snowmelt only in August (1980 and 1997). In all years, >90% of the effective snow is produced by the end of September.

https://doi.org/10.5194/esurf-2022-58
Preprint. Discussion started: 16 November 2022

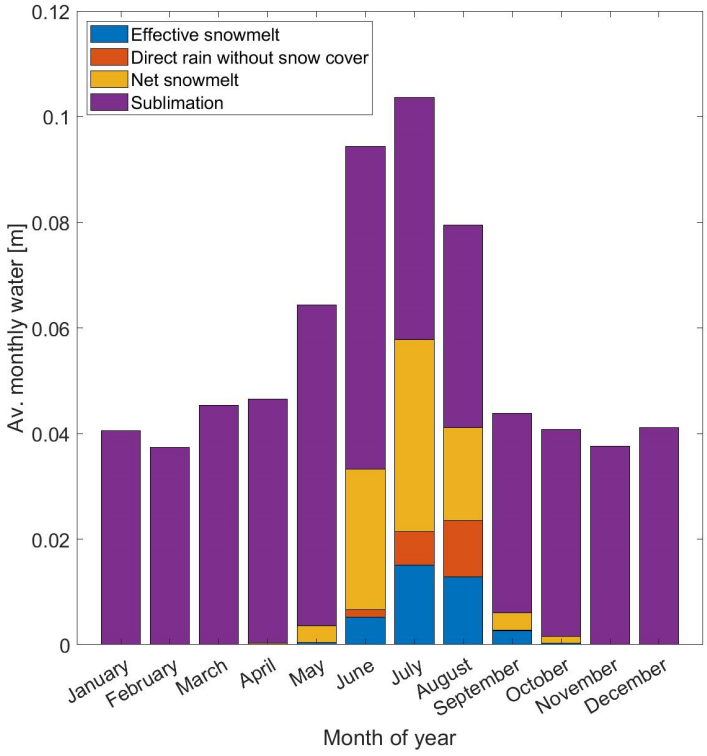

Figure 6: Average modeled monthly water fluxes for the period 1959-2020.

The flexibility of the model setup enables the simulation of opposite north and south facing rock slopes to test the effect of topographic aspect on runoff regime. Model results show that both north and south facing rock slopes experience complete melting of snow cover by late summer which is in agreement with field observations. Similar volumes of total runoff are produced, with negligible differences due to different sublimation rates. Interestingly, the annual effective snowmelt on south facing rock slopes is 48% greater on average than on north facing slopes (Fig. 7). The reason for this is twofold: first, while the duration of effective snowmelt on south facing rock-slopes ranges from May to October, the effective snowmelt on the north face is limited to June to September (fig. 7). This is related to the limited duration of the positive rock surface T on the north aspect (Fig. 7) and the longer persistence of ice crust at the base of the snowpack.

https://doi.org/10.5194/esurf-2022-58
Preprint. Discussion started: 16 November 2022

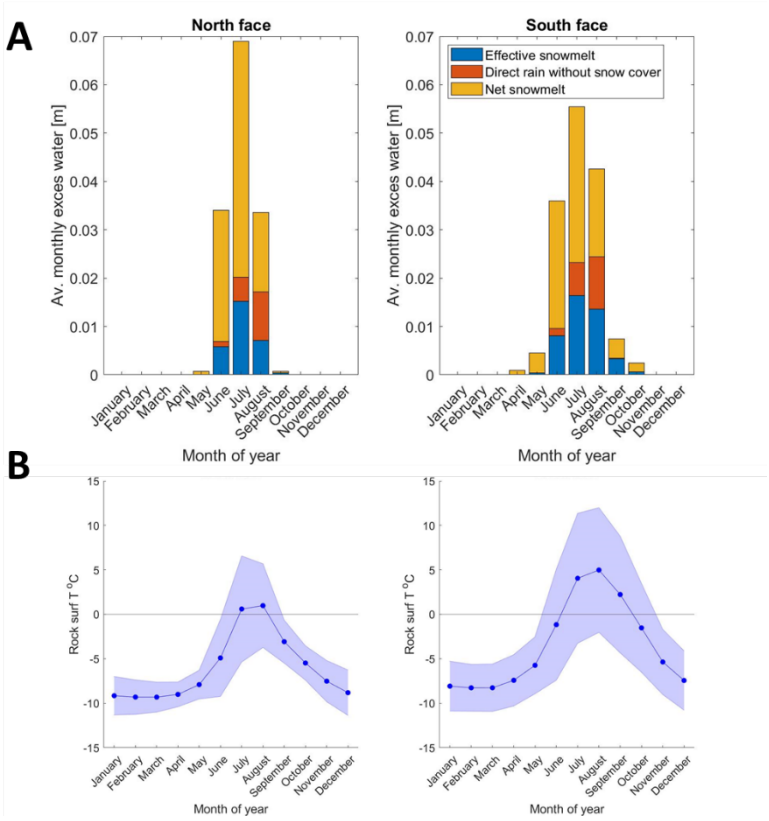

Figure 7: North vs. South comparison - A) Comparison of average monthly distribution of water fluxes in north and south facing rock slopes at an elevation of 3900 m a.s.l. Note that the annual effective snowmelt on south facing rock slopes is 48% greater on average than on north facing slopes, while the duration of effective snowmelt on south facing rock-slopes range from May to October, the effective snowmelt on the north face is limited to June to September. B) Average surface T in north and south facing rock slopes at an elevation of 3900 m a.s.l. Blue area shows the standard deviation of monthly surface T.

4.4. Modeling elevation change

The S2M-SAFRAN dataset for the Mont-Blanc massif is available at elevation steps of 300 m. We compared our model simulation results for the AdM SE face with the same settings at elevations of 2700, 3000, 3300, 3600, 3900, 4200, 4500, and 4800 m a.s.l. These simulations give a better understanding of the thermal dynamics along the entire permafrost affected mountain flank and the changes in effective snowmelt and water availability for infiltration. To broaden the analysis, we also modeled the effect of elevation change on a north facing slope. Our results show that for south facing rock slopes, snowmelt is the main source of water for infiltration in elevations above 3600 m a.s.l. From 3600 m to 2700 m, direct input of rainfall and total snowmelt volumes increase rapidly, while the effective snowmelt increase at a more gradual rate (Fig. 8). At these lower elevations, where direct rainfall is dominant, effective snowmelt input precedes rainfall by ~1 month on average (Fig. 8A). Above 3300 m, sublimation is the dominant process of snow mass loss. The availability of water for infiltration, either by snowmelt or direct rainfall, occurs sooner at lower elevations. Above 3600 m, water is available for infiltration in June and

https://doi.org/10.5194/esurf-2022-58
Preprint. Discussion started: 16 November 2022

as early as April at elevation of 2700 – 3000 m. A comparison with the same elevations on a north face (Fig. 9) shows that at elevations <3000 m, fluxes are similar on both aspects. At higher elevations, the ratio of water availability between north to south increases while the water fluxes magnitudes decrease.

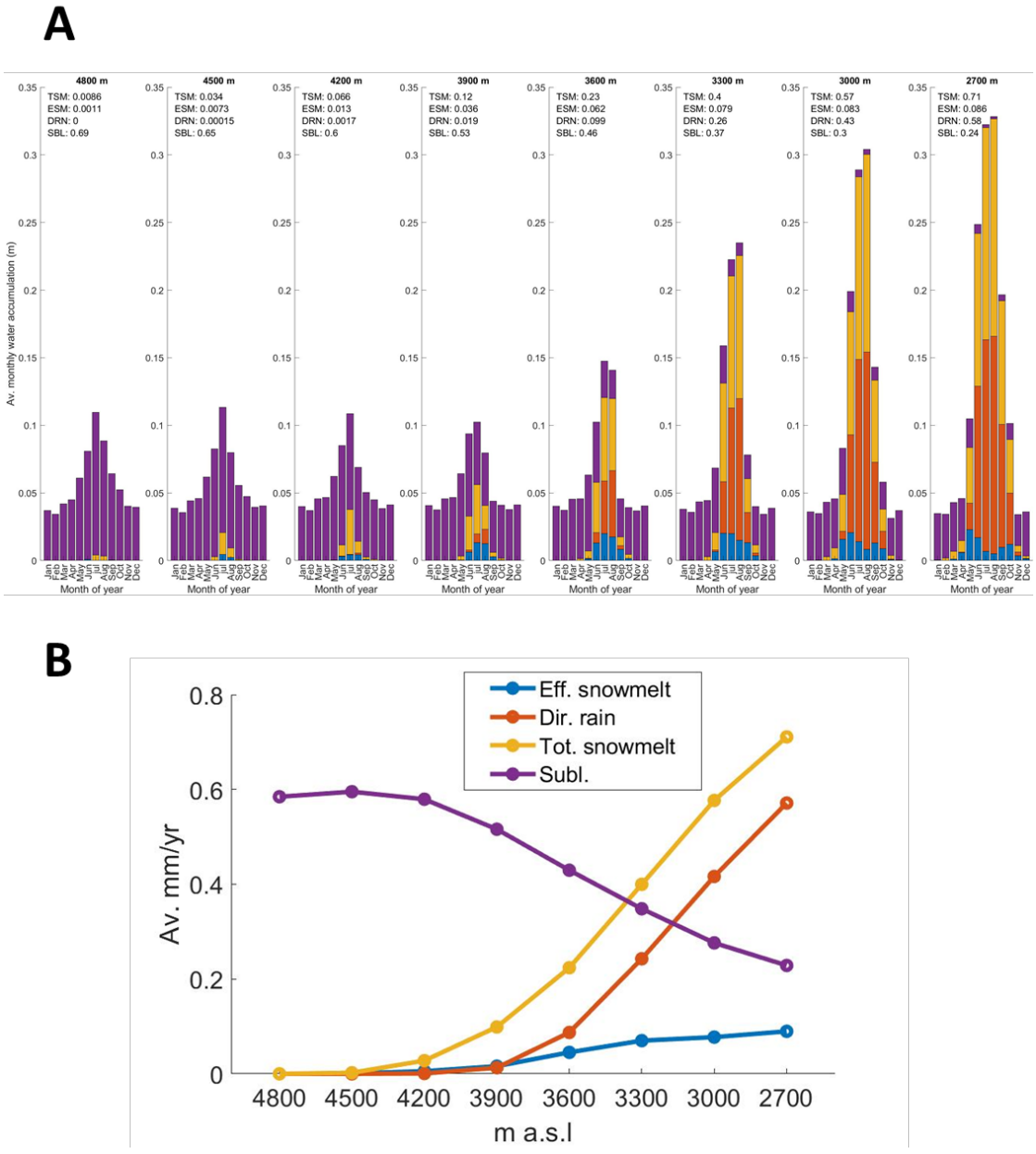

275 **Figure 8: Comparison of average monthly distribution of water fluxes at elevations ranging from 4800 to 2700 m a.s.l. - A) Comparison of average monthly distribution of water fluxes, at elevations of 4800, 4500, 4200, 3900, 3600, 3300, 3000 and 2700 m a.s.l. on SE facing rock slope. TSM: total snowmelt; ESM: effective snowmelt; DRN: direct rainfall; SBL: sublimation. B) Average annual fluxes in each of the modeled elevations between 4800-2700 m a.s.l. on SE facing rock slopes. Note the rapid increase in water availability from rainfall input below 3900 m.**

https://doi.org/10.5194/esurf-2022-58
Preprint. Discussion started: 16 November 2022

5 Discussion

5.1. Snow depth

Our results show a robust inverse relation between slope angle and snow accumulation depth, which is in agreement with results of previous studies (Sommer et al., 2015; Blöschl et al., 1991; Winstral et al., 2002; Gruber Schmid and Sardemann, 2003; Haberkorn et al., 2015). We acknowledge the observed variance in snow accumulation depth for a given slope (Fig. 2). This variance is interesting by itself since it might point to additional environmental factors that control snow accumulation (Wirz et al., 2011; Lehning et al., 2011), most likely local micro-topographic and micro-climatic factors. For example, micro-topography of the rock surface can influence local wind dynamics and snow redistribution (Winstral et al., 2002). The rock slope roughness can affect friction with the snowpack surface and support its stability. Local shading can affect the thermal regime and mechanical characteristics of the snowpack (Vionnet et al., 2012). Further research using higher temporal and spatial resolution is needed to decipher the influence of slope characteristics other than slope angle on snow accumulation in steep slopes.

5.2. Model applications and flexibility of the S2M-SAFRAN dataset

On-site meteorological measurements in high mountain environments are difficult to setup and maintain and data is often discontinuous and limited. Remote sensing data from satellites and global climate models can be used to produce local climatic time series, however their spatial resolution is insufficient for rock slope scale processes. We show that the use of the S2M-SAFRAN meteorological dataset can overcome some of these limitations, especially in locations where an *in-situ* meteorological stations is available nearby to improve its accuracy. Once calibrated, the CryoGrid model can benefit from the resolution of the S2M-SAFRAN data that is divided into elevation steps of 300 m. The S2M-SAFRAN data is available for other mountain ranges in the Alps, Pyrenees (*e.g.* López-Moreno et al., 2020) and Corsica and our approach could be extended if enough field data is available for validation (*i.e.*, surface T and/or snow depth).

The CryoGrid community model is a useful tool for studying near surface thermal and hydrological processes in steep mountainous landscape. However, although the model allows considerations of lateral drainage it is spatially limited to one-dimensional configuration and over simplify 3D subsurface thermal and hydrological processes. 3D hydrogeological models that can account for lateral flow, heat advection and various saturation levels do exist. However, these models, in addition to often being closed sourced and costly, rarely include modules for simulating the complex processes in the snowpack and the interactions with meteorological and topographical conditions. We thus suggest that a complete model of the thermal and hydrological processes in mountainous periglacial and/or permafrost-affected landscapes can benefit from a coupling of the output of an energy balance + snow hydrology model, such as CryoGrid, with a 3D hydrogeological model of mass and heat transfer.

https://doi.org/10.5194/esurf-2022-58
Preprint. Discussion started: 16 November 2022


Earth Surface Dynamics Discussions
Open Access
EGU

5.3. Potential snowmelt and water balance

Our results fill a major knowledge gap in the field of steep mountain slopes with permafrost related to the availability of water for infiltration. We demonstrate some of the known complexity of the environmental controls on water availability in high elevation steep rock slopes, such as the formation of an ice crust layer that can profoundly lower the local rock surface infiltration capacity (Woo and Heron, 1981; Woo et al., 1982; Marsh, 2005; Phillips et al., 2016). We found sublimation to be the most dominant process of snowpack mass loss. Accurate modeling of sublimation in steep - high alpine terrain is highly complex and field measurements are rare, however, previous studies pointed out the importance of sublimation in the alpine snowpack mass balance (Strasser et al., 2008; MacDonald et al., 2010). We found sublimation rate to be sensitive to surface roughness length – a parameter that describes the efficiency of energy transfer (*i.e.* latent heat of sublimation) between the air and the snowpack surface. We tested the sensitivity of sublimation rates to a wide range of roughness length (Table 1) values (1×10^{-4} - 2×10^{-2} m) and found that and although sublimation changed significantly it remained the most dominant flux of snow mass loss. We show that effective snowmelt is the main source of water availability to the rock surface in steep high elevated rock slopes and that at intermediate elevations, *i.e.* 3600-3900 m a.s.l in our case study, a transition occurs from snowmelt-dominated to rainfall-dominated water availability (Fig. 8). A high rockfall frequency in such a permafrost-affected site was recently demonstrated by Mourey et al. (2022) in the Mont-Blanc massif. We compared the influence of elevation on water balance in N and S facing hillslopes (Fig. 9A) and found that differences are more prominent at higher elevations – as S facing rock slopes receive more water input in compare with N facing (Fig. 9B). This results from the interplay of snow cover dynamics which in turn influence snowmelt and rock surface exposure to direct rain, in addition to differences in ice crust formation. Considering the connectivity in the slope length scale, some of the surface runoff that is generated from snowmelt at high elevation in spring and early summer, due to sealing of the rock surface with an ice crust, may reach a lower elevation where the rock is not sealed and amplify the observed increase in water contribution at the transition elevation.

In this contribution, we focus on the availability of water for infiltration at the rock surface; however, the actual infiltration rate depends on the infiltration capacity of the rock. Any water fluxes that exceed the infiltration capacity will not infiltrate and flow as runoff. Maréchal et al. (1999) estimated the hydraulic conductivity of the crystalline rock that composes the AdM to 10^{-8} m/s. Since the hydraulic conductivity of the granitic rock is much lower (Bear, 1988), the actual value is controlled by the fractures in the rock – their density, aperture and connectivity. Utilizing an empirical equation suggested by Kiraly (1969, 1994) which accounts for fracture density and aperture, and using conservative values of fracture density of 2 m^{-1} and fracture aperture of 0.5 mm, we get a value that is two orders of magnitude higher (6×10^{-6} m/s) than that of Maréchal et al. (1999). Looking at our results, if we convert our model results of effective snowmelt to the common units for hydraulic conductivity of m/s we find that 95% of the effective snowmelt occur at rates that fall between these estimations (10×10^{-8} - 6×10^{-6} m/s), thus making infiltration capacity (or hydraulic conductivity) an important parameter for estimation of infiltration in steep fractured rock wall.

https://doi.org/10.5194/esurf-2022-58
Preprint. Discussion started: 16 November 2022

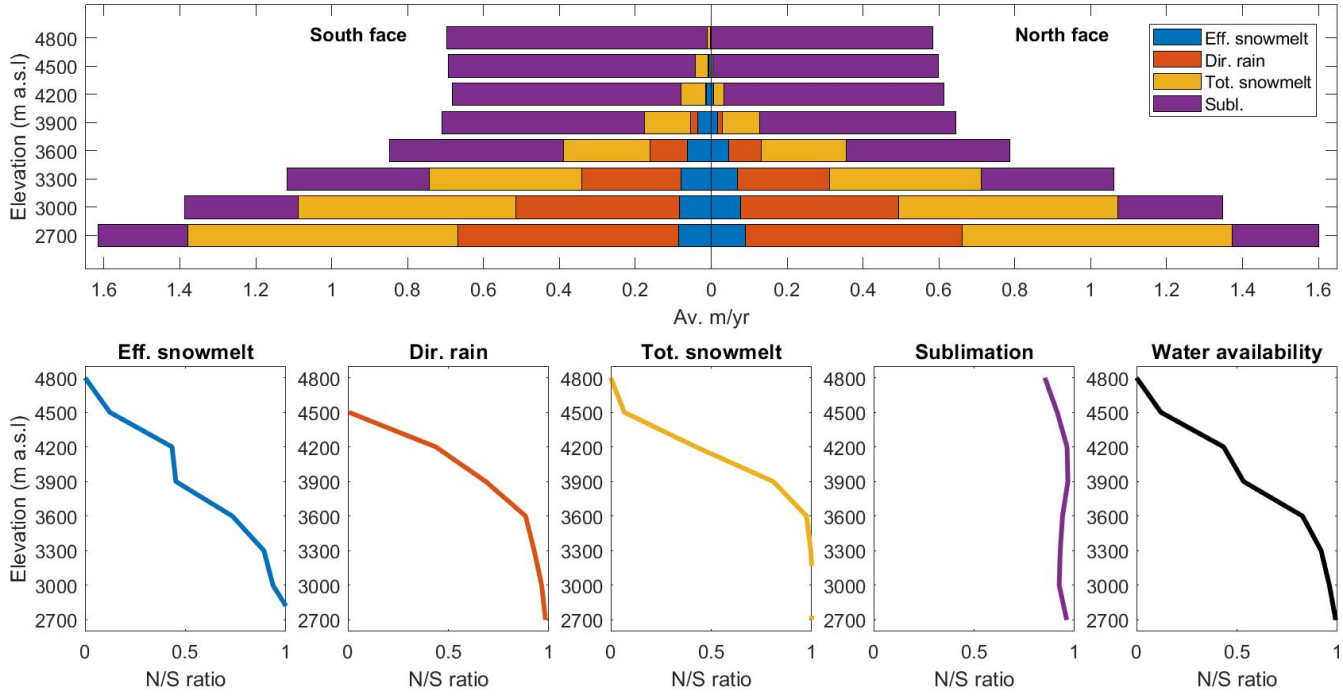

Figure 9: North vs. South comparison of average monthly distribution of water fluxes at elevations of 2700 – 4800 m a.s.l. – Top: Comparison of average annual water fluxes, at elevations of 4800, 4500, 4200, 3900, 3600, 3300, 3000 and 2700 m a.s.l. on north (left) and south (right) facing rock slopes. Bottom: The ratio between north to south of each component of the water fluxes described above, in each of the modeled elevation. A value of 1 represents equal flux on both aspects, and values decreasing toward 0 represent larger ratio between S to N face (for example, a value of 0.5 corresponds to ×2 higher flux on the S face). The bottom right image shows the flux of net water availability at the rock surface, that is available for infiltration (effective snowmelt + direct rain). Note that at elevations <3000 m a.s.l fluxes are similar on both aspects and the ratio decreases at higher elevations but the water fluxes magnitudes decrease.

5.4. Implications of results

The new information we present on the timing and quantity of water input at the rock surface can be used to improve the understanding of thermal, hydrogeological and mechanical processes in steep mountain rock slopes, such as water pressure (Matsuoka, 2019; D'Amato et al., 2016) and permafrost degradation that was previously shown to be linked with a decrease in the mechanical stability of steep rock slopes and initiation failure and rock fall occurrence (Gruber et al., 2004; Gruber and Haeberli, 2007; Ravanel and Deline, 2015).

Our model setup using the CryoGrid community model can be applied in other steep alpine rock slopes to assess water availability and risk assessments from thawing related rock failure.

We hypothesize that rock slopes at elevations of 3600-3900 m a.s.l., where we observe a sharp transition in water availability (Fig. 8), are especially sensitive to climate change. Our simulations show that water availability increases rapidly below these elevations due to high rates of direct rainfall. In a scenario that air temperatures and the intensity of summer rains increases due to climate change (Pepin et al., 2022; Pepin, N. et al., 2015; Biskaborn et al., 2019), and the observed nonlinear trend of

https://doi.org/10.5194/esurf-2022-58
Preprint. Discussion started: 16 November 2022

Earth Surface Dynamics Discussions
Open Access
EGU

water input is 'shifted' upwards to higher elevations, we expect that higher elevation permafrost-affected slopes will experience an abrupt increase in water input from rainfall which could prompt permafrost degradation and mechanical destabilization. This effect will be more prominent at the transition elevations that will change from snowmelt- to rainfall-dominated input, and less in higher elevations that will remain snowmelt-dominated. Field observations support this hypothesis: topographic analysis of data from 209 rockfalls in the Mont-Blanc massif between 2007 and 2015 (Legay et al., 2021) show that rockfalls on S, E and W facing rock walls occur mostly at elevation of 3300-3600 m, and at elevation of 3000-3300 m a.s.l on N facing rock walls (Fig. 10), suggesting that elevation dependent climate change (Pepin et al., 2022; Pepin, N. et al., 2015) is responsible for the observed peak in rockfalls occurrence at the water availability transition elevation. During the 2003 and 2015 summer heatwaves in the Mont-Blanc massif, Ravanel et al. (2017) showed that numerous rock falls were initiated at average elevations of 3300 m a.s.l and 3600 m a.s.l on north and south faces respectfully, and that hydrostatic pressure related to thaw or extreme rain, and advective heat transport at depth by water percolation along discontinuities are likely rockfall triggering factors. The lower elevation of the maximum rockfall occurrence on the north face could be related to the influence of the lower snowline and related processes which are not accounted in the simplified aspect conversion of our model. 3600 m a.s.l. was also reported as the lower boundary of continuous stable occurrence of permafrost in the Mont-Blanc massif (Magnin et al., 2015a). Below 3600 m rockwall permafrost was shown to occur locally from an elevation of 1900 m a.s.l with strong dependency on local structural settings and aspect (Magnin et al., 2015a). In addition, our results could be used in parameterization and forcing data in further modeling of subsurface hydrogeological processes and larger spatial scale analysis, and to study watershed hydrology in high mountain environments and the role of heat advection by water infiltration through rock fractures.

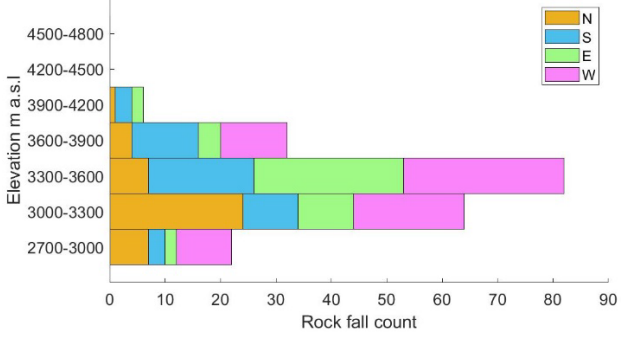

Figure 10: Topographic analysis of rockfalls documented by Legay et al. (2021) in the Mont-Blanc massif between 2007 and 2015. Rock falls are most common at elevations of 3300-3600 m a.s.l. This trend is consistent for S, E and W facing slopes. On N facing slopes, highest occurrence is at the elevation range of 3000-3300 m.

6 Conclusions

The importance of water in driving surface processes in steep periglacial landscapes is recognized by numerous studies. However, the complexity of the physical processes related to snow hydrology and challenges in data acquisition in these

https://doi.org/10.5194/esurf-2022-58
Preprint. Discussion started: 16 November 2022

extreme environments result in a major knowledge gap in the availability of water at the slope surface. Using field measurement and numerical modeling, we simulated the energy balance and hydrological fluxes in a steep high-elevated permafrost-affected rock slope at Aiguille du Midi, in the Mont-Blanc massif. Our results provide new information about water balance at the surface of steep rock slopes. This includes the quantity and temporal distribution of the effective snowmelt that is available for infiltration in addition to input from rainfall and mass losses by sublimation and runoff. Our results provide essential information to risk assessments of rock falls and rock avalanches that are often triggered by water flow in fractures. We highlight the following conclusions:

- The combined application of the S2M-SAFRAN dataset with the CryoGrid community model that we present here is a powerful tool to study cryogenic and hydrologic processes in high alpine landscapes. Such capabilities are presented in this study in the comparison of various aspects, slope angles and elevations.
- We estimate that in our study site, in a steep rock slope on the SE face of AdM, only ~25% of the snowfall accumulates. The remaining ~75% is redistributed by wind and gravity. We also found that snow accumulation thickness is inversely correlated with surface slopes between 40° to 70°.
- Snowmelt occurs between late spring and late summer, and most of it does not reach the rock surface due to a formation of an impermeable ice layer at the base of the snowpack. The annual effective snowmelt that is available for infiltration is highly variable and ranges over a factor of six, between 0.05 and 0.28 m during the period 1959-2021. The timing of the first effective snowmelt in the year ranges between May-August, and effective snowmelt ends before October; it precedes the first rainfall input by one month on average.
- Sublimation is the main process of snowpack mass loss in our study site.
- Results of model simulations at varying elevations show that effective snowmelt is the main source of potential water for infiltration at elevation >3600 m a.s.l. Below 3600 m, direct rainfall is becoming more dominant. The change from snowmelt-dominated to rainfall-dominated water availability is nonlinear and characterized by a rapid increase in water availability for infiltration. We suggest that this transition elevation is highly sensitive to climate change, as permafrost-affected slopes experience an abrupt increase in water input that can initiate rock failure.

Author contributions

MBA and FM conceptualized and designed the research. MBA analyzed the data. MBA, FM, JB, EM, JB performed field work. SW developed the model and wrote the code. MBA, FM, JB, SW, LR and PD wrote the manuscript.

Acknowledgements and data availability

This study is funded by the ANR-19-CE01-0018 WISPER project. We thank the Compagnie du Mont-Blanc and the Aiguille du Midi station staff for their support in access to the site.

Data used in this paper are available at https://zenodo.org/record/7224692#.Y0--OnaxWUk

https://doi.org/10.5194/esurf-2022-58
Preprint. Discussion started: 16 November 2022

References

Allen, S. K., Gruber, S., and Owens, I. F.: Exploring steep bedrock permafrost and its relationship with recent slope failures in the Southern Alps of New Zealand, Permafr. Periglac. Process., 20, 345–356, https://doi.org/10.1002/ppp.658, 2009.

Bear, J.: Dynamics of Fluids in Porous Media, Courier Corporation, 806 pp., 1988.

Biskaborn, B. K., Smith, S. L., Noetzli, J., Matthes, H., Vieira, G., Streletskiy, D. A., Schoeneich, P., Romanovsky, V. E., Lewkowicz, A. G., Abramov, A., Allard, M., Boike, J., Cable, W. L., Christiansen, H. H., Delaloye, R., Diekmann, B., Drozdov, D., Etzelmüller, B., Grosse, G., Guglielmin, M., Ingeman-Nielsen, T., Isaksen, K., Ishikawa, M., Johansson, M., Johannsson, H., Joo, A., Kaverin, D., Kholodov, A., Konstantinov, P., Kröger, T., Lambiel, C., Lanckman, J. P., Luo, D., Malkova, G., Meiklejohn, I., Moskalenko, N., Oliva, M., Phillips, M., Ramos, M., Sannel, A. B. K., Sergeev, D., Seybold, C., Skryabin, P., Vasiliev, A., Wu, Q., Yoshikawa, K., Zheleznyak, M., and Lantuit, H.: Permafrost is warming at a global scale, Nat. Commun., 10, 1–11, https://doi.org/10.1038/s41467-018-08240-4, 2019.

Blöschl, G., Kirnbauer, R., and Gutknecht, D.: Distributed Snowmelt Simulations in an Alpine Catchment: 1. Model Evaluation on the Basis of Snow Cover Patterns, Water Resour. Res., 27, 3171–3179, https://doi.org/10.1029/91WR02250, 1991.

D'Amato, J., Hantz, D., Guerin, A., Jaboyedoff, M., Baillet, L., and Mariscal, A.: Influence of meteorological factors on rockfall occurrence in a middle mountain limestone cliff, Nat. Hazards Earth Syst. Sci., 16, 719–735, https://doi.org/10.5194/nhess-16-719-2016, 2016.

Draebing, D., Krautblatter, M., and Dikau, R.: Interaction of thermal and mechanical processes in steep permafrost rock walls: A conceptual approach, Geomorphology, 226, 226–235, https://doi.org/10.1016/j.geomorph.2014.08.009, 2014.

Durand, Y., Brun, E., Merindol, L., Guyomarc'h, G., Lesaffre, B., and Martin, E.: A meteorological estimation of relevant parameters for snow models, Ann. Glaciol., 18, 65–71, https://doi.org/10.3189/S0260305500011277, 1993.

Eppes, M. C. and Keanini, R.: Mechanical weathering and rock erosion by climate-dependent subcritical cracking, Rev. Geophys., 55, 470–508, https://doi.org/10.1002/2017RG000557, 2017.

Evans, I. S.: An integrated system of terrain analysis and slope mapping, Z. Geomorphol., 36, 274–295, 1980.

Fischer, L., Amann, F., Moore, J. R., and Huggel, C.: Assessment of periglacial slope stability for the 1988 Tschierva rock avalanche (Piz Morteratsch, Switzerland), Eng. Geol., 116, 32–43, https://doi.org/10.1016/j.enggeo.2010.07.005, 2010.

French, H. M.: The Periglacial Environment, https://doi.org/10.1002/9781119132820, 2017.

Gruber, S. and Haeberli, W.: Permafrost in steep bedrock slopes and its temperatures-related destabilization following climate change, J. Geophys. Res. Earth Surf., 112, 1–10, https://doi.org/10.1029/2006JF000547, 2007.

Gruber, S., Hoelzle, M., and Haeberli, W.: Rock-wall temperatures in the Alps: Modelling their topographic distribution and regional differences, Permafr. Periglac. Process., 15, 299–307, https://doi.org/10.1002/ppp.501, 2004.

Gruber Schmid, U. and Sardemann, S.: High-frequency avalanches: release area characteristics and run-out distances, Cold Reg. Sci. Technol., 37, 439–451, https://doi.org/10.1016/S0165-232X(03)00083-1, 2003.

https://doi.org/10.5194/esurf-2022-58
Preprint. Discussion started: 16 November 2022

Haberkorn, A., Phillips, M., Kenner, R., Rhyner, H., Bavay, M., Galos, S. P., and Hoelzle, M.: Thermal Regime of Rock and its Relation to Snow Cover in Steep Alpine Rock Walls: Gemsstock, Central Swiss Alps, Geogr. Ann. Ser. Phys. Geogr., 97, 579–597, https://doi.org/10.1111/geoa.12101, 2015.

Haberkorn, A., Wever, N., Hoelzle, M., Phillips, M., Kenner, R., Bavay, M., and Lehning, M.: Distributed snow and rock temperature modelling in steep rock walls using Alpine3D, Cryosphere, 11, 585–607, https://doi.org/10.5194/tc-11-585-2017, 2017.

Haeberli, W. and Gruber, S.: Global Warming and Mountain Permafrost, in: Permafrost Soils, vol. 16, edited by: Margesin, R., Springer Berlin Heidelberg, Berlin, Heidelberg, 205–218, https://doi.org/10.1007/978-3-540-69371-0_14, 2009.

Haeberli, W., Noetzli, J., Arenson, L., Delaloye, R., Gärtner-Roer, I., Gruber, S., Isaksen, K., Kneisel, C., Krautblatter, M., and Phillips, M.: Mountain permafrost: development and challenges of a young research field, J. Glaciol., 56, 1043–1058, https://doi.org/10.3189/002214311796406121, 2010.

Hales, T. C. and Roering, J. J.: Climatic controls on frost cracking and implications for the evolution of bedrock landscapes, J. Geophys. Res., 112, F02033–F02033, https://doi.org/10.1029/2006JF000616, 2007.

Hallet, B., Walder, J. S., and Stubbs, C. W.: Weathering by segregation ice growth in microcracks at sustained subzero temperatures: Verification from an experimental study using acoustic emissions, Permafr. Periglac. Process., 2, 283–300, https://doi.org/10.1002/ppp.3430020404, 1991.

Hasler, A., Gruber, S., Font, M., and Dubois, A.: Advective heat transport in frozen rock clefts: Conceptual model, laboratory experiments and numerical simulation, Permafr. Periglac. Process., 22, 378–389, https://doi.org/10.1002/ppp.737, 2011.

Hersbach, H., Bell, B., Berrisford, P., Hirahara, S., Horányi, A., Muñoz-Sabater, J., Nicolas, J., Peubey, C., Radu, R., Schepers, D., Simmons, A., Soci, C., Abdalla, S., Abellan, X., Balsamo, G., Bechtold, P., Biavati, G., Bidlot, J., Bonavita, M., Chiara, G., Dahlgren, P., Dee, D., Diamantakis, M., Dragani, R., Flemming, J., Forbes, R., Fuentes, M., Geer, A., Haimberger, L., Healy, S., Hogan, R. J., Hólm, E., Janisková, M., Keeley, S., Laloyaux, P., Lopez, P., Lupu, C., Radnoti, G., Rosnay, P., Rozum, I., Vamborg, F., Villaume, S., and Thépaut, J.: The ERA5 global reanalysis, Q. J. R. Meteorol. Soc., 146, 1999–2049, https://doi.org/10.1002/qj.3803, 2020.

Hood, J. L. and Hayashi, M.: Assessing the application of a laser rangefinder for determining snow depth in inaccessible alpine terrain, Hydrol. Earth Syst. Sci., 14, 901–910, https://doi.org/10.5194/hess-14-901-2010, 2010.

Huggel, C., Allen, S., Deline, P., Fischer, L., Noetzli, J., and Ravanel, L.: Ice thawing, mountains falling-are alpine rock slope failures increasing, Geol. Today, 28, 98–104, https://doi.org/10.1111/j.1365-2451.2012.00836.x, 2012.

Kiraly, L.: Groundwater flow in fractured rocks: models and reality: with 15 figures (with author annotations), in: 14. Mintrop-Seminar über Interpretationsstrategien in Exploration und Produktion, 1–21, 1994.

Kiraly, Laszlo.: Anisotropie et hétérogénéité de la perméabilité dans les calcaires fissurés (Anisotropy and heterogeneity of permeability in fractured limestones), Eclogae Geol. Helvetiae, 62, 613–619, 1969.

Krautblatter, M., Funk, D., and Günzel, F. K.: Why permafrost rocks become unstable: A rock-ice-mechanical model in time and space, Earth Surf. Process. Landf., 38, 876–887, https://doi.org/10.1002/esp.3374, 2013.

Legay, A., Magnin, F., and Ravanel, L.: Rock temperature prior to failure: Analysis of 209 rockfall events in the Mont Blanc massif (Western European Alps), Permafr. Periglac. Process., 32, 520–536, https://doi.org/10.1002/ppp.2110, 2021.

Lehning, M., Grünewald, T., and Schirmer, M.: Mountain snow distribution governed by an altitudinal gradient and terrain roughness: ROUGHNESS CONTROL ON MOUNTAIN SNOW, Geophys. Res. Lett., 38, n/a-n/a, https://doi.org/10.1029/2011GL048927, 2011.

Leloup, P. H., Arnaud, N., Sobel, E. R., and Lacassin, R.: Alpine thermal and structural evolution of the highest external crystalline massif: The Mont Blanc: EXHUMATION OF THE MONT BLANC MASSIF, Tectonics, 24, n/a-n/a, https://doi.org/10.1029/2004TC001676, 2005.

López-Moreno, J. I., Soubeyroux, J. M., Gascoin, S., Alonso-Gonzalez, E., Durán-Gómez, N., Lafaysse, M., Vernay, M., Carmagnola, C., and Morin, S.: Long-term trends (1958–2017) in snow cover duration and depth in the Pyrenees, Int. J. Climatol., 40, 6122–6136, https://doi.org/10.1002/joc.6571, 2020.

MacDonald, M. K., Pomeroy, J. W., and Pietroniro, A.: On the importance of sublimation to an alpine snow mass balance in the Canadian Rocky Mountains, Hydrol. Earth Syst. Sci., 14, 1401–1415, https://doi.org/10.5194/hess-14-1401-2010, 2010.

Magnin, F. and Josnin, J.-Y.: Water Flows in Rockwall Permafrost : a Numerical Approach Coupling Hydrological and Thermal Processes, J. Geophys. Res. Earth Surf., 2021.

Magnin, F., Brenning, A., Bodin, X., Deline, P., and Ravanel, L.: Modélisation statistique de la distribution du permafrost de paroi : application au massif du Mont Blanc, Géomorphologie Relief Process. Environ., 21, 145–162, https://doi.org/10.4000/geomorphologie.10965, 2015a.

Magnin, F., Deline, P., Ravanel, L., Noetzli, J., and Pogliotti, P.: Thermal characteristics of permafrost in the steep alpine rock walls of the Aiguille du Midi (Mont Blanc Massif, 3842 m a.s.l), Cryosphere, 9, 109–121, https://doi.org/10.5194/tc-9-109-2015, 2015b.

Magnin, F., Westermann, S., Pogliotti, P., Ravanel, L., Deline, P., and Malet, E.: Snow control on active layer thickness in steep alpine rock walls (Aiguille du Midi, 3842 m a.s.l., Mont Blanc massif), Catena, 149, 648–662, https://doi.org/10.1016/j.catena.2016.06.006, 2017.

Maréchal, J. C., Perrochet, P., and Tacher, L.: Long-term simulations of thermal and hydraulic characteristics in a mountain massif: The Mont Blanc case study, French and Italian Alps, Hydrogeol. J., 7, 341–354, https://doi.org/10.1007/s100400050207, 1999.

Marsh, P.: Water Flow through Snow and Firn, in: Encyclopedia of Hydrological Sciences, edited by: Anderson, M. G. and McDonnell, J. J., John Wiley & Sons, Ltd, Chichester, UK, hsa167, https://doi.org/10.1002/0470848944.hsa167, 2005.

Matsuoka, N.: A multi-method monitoring of timing, magnitude and origin of rockfall activity in the Japanese Alps, Geomorphology, 336, 65–76, https://doi.org/10.1016/j.geomorph.2019.03.023, 2019.

Mineo, S. and Pappalardo, G.: Rock Emissivity Measurement for Infrared Thermography Engineering Geological Applications, Appl. Sci., 11, 3773, https://doi.org/10.3390/app11093773, 2021.

Mott, R., Schirmer, M., Bavay, M., Grünewald, T., and Lehning, M.: Understanding snow-transport processes shaping the mountain snow-cover, Cryosphere, 4, 545–559, https://doi.org/10.5194/tc-4-545-2010, 2010.

Mourey, J., Lacroix, P., Duvillard, P.-A., Marsy, G., Marcer, M., Malet, E., and Ravanel, L.: Multi-method monitoring of rockfall activity along the classic route up Mont Blanc (4809 m a.s.l.) to encourage adaptation by mountaineers, Nat. Hazards Earth Syst. Sci., 22, 445–460, https://doi.org/10.5194/nhess-22-445-2022, 2022.

525 Myhra, K. S., Westermann, S., and Etzelmüller, B.: Modelled Distribution and Temporal Evolution of Permafrost in Steep Rock Walls Along a Latitudinal Transect in Norway by CryoGrid 2D, Permafr. Periglac. Process., 28, 172–182, https://doi.org/10.1002/ppp.1884, 2017.

Naseer, A., Koike, T., Rasmy, M., Ushiyama, T., and Shrestha, M.: Distributed Hydrological Modeling Framework for Quantitative and Spatial Bias Correction for Rainfall, Snowfall, and Mixed-Phase Precipitation Using Vertical Profile of
530 Temperature, J. Geophys. Res. Atmospheres, 124, 4985–5009, https://doi.org/10.1029/2018JD029811, 2019.

Pepin, N., Bradley, R. S., Diaz, H. F., Baraer, M., Caceres, E. B., Forsythe, N., Fowler, H., Greenwood, G., Hashmi, M. Z., Liu, X. D., Miller, J. R., Ning, L., Ohmura, A., Palazzi, E., Rangwala, I., Schöner, W., Severskiy, I., Shahgedanova, M., Wang, M. B., Williamson, S. N., and Yang, D. Q.: Elevation-dependent warming in mountain regions of the world, Nat. Clim. Change, 5, 424–430, https://doi.org/10.1038/nclimate2563, 2015.

535 Pepin, N. C., Arnone, E., Gobiet, A., Haslinger, K., Kotlarski, S., Notarnicola, C., Palazzi, E., Seibert, P., Serafin, S., Schöner, W., Terzago, S., Thornton, J. M., Vuille, M., and Adler, C.: Climate Changes and Their Elevational Patterns in the Mountains of the World, Rev. Geophys., 60, https://doi.org/10.1029/2020RG000730, 2022.

Phillips, M., Haberkorn, A., Draebing, D., Krautblatter, M., Rhyner, H., and Kenner, R.: Seasonally intermittent water flow through deep fractures in an Alpine Rock Ridge: Gemsstock, Central Swiss Alps, Cold Reg. Sci. Technol., 125, 117–127,
540 https://doi.org/10.1016/j.coldregions.2016.02.010, 2016.

Phillips, M., Haberkorn, A., and Rhyner, H.: Snowpack characteristics on steep frozen rock slopes, Cold Reg. Sci. Technol., 141, 54–65, https://doi.org/10.1016/j.coldregions.2017.05.010, 2017.

Ravanel, L. and Deline, P.: Climate influence on rockfalls in high-alpine steep rockwalls: The north side of the aiguilles de chamonix (mont blanc massif) since the end of the "Little Ice Age," Holocene, 21, 357–365,
545 https://doi.org/10.1177/0959683610374887, 2011.

Ravanel, L. and Deline, P.: A network of observers in the Mont-Blanc massif to study rockfall from high Alpine rockwalls, Geogr. Fis. E Din. Quat., 151–158, https://doi.org/10.4461/GFDQ.2013.36.12, 2013.

Ravanel, L. and Deline, P.: Rockfall Hazard in the Mont Blanc Massif Increased by the Current Atmospheric Warming, in: Engineering Geology for Society and Territory - Volume 1, edited by: Lollino, G., Manconi, A., Clague, J., Shan, W., and
550 Chiarle, M., Springer International Publishing, Cham, 425–428, https://doi.org/10.1007/978-3-319-09300-0_81, 2015.

Ravanel, L., Magnin, F., and Deline, P.: Impacts of the 2003 and 2015 summer heatwaves on permafrost-affected rock-walls in the Mont Blanc massif, Sci. Total Environ., 609, 132–143, https://doi.org/10.1016/j.scitotenv.2017.07.055, 2017.

Schmidt, J. U., Etzelmüller, B., Schuler, T. V., Magnin, F., Boike, J., Langer, M., and Westermann, S.: Surface temperatures and their influence on the permafrost thermal regime in high-Arctic rock walls on Svalbard, Cryosphere, 15, 2491–2509,
555 https://doi.org/10.5194/tc-15-2491-2021, 2021.

Sokratov, S. A. and Sato, A.: The effect of wind on the snow cover, Ann. Glaciol., 32, 116–120, https://doi.org/10.3189/172756401781819436, 2001.

Sommer, C. G., Lehning, M., and Mott, R.: Snow in a Very Steep Rock Face: Accumulation and Redistribution During and After a Snowfall Event, Front. Earth Sci., 3, https://doi.org/10.3389/feart.2015.00073, 2015.

560 Sommerfeld, R. A. and Rocchio, J. E.: Permeability measurements on new and equitemperature snow, Water Resour. Res., 29, 2485–2490, https://doi.org/10.1029/93WR01071, 1993.

https://doi.org/10.5194/esurf-2022-58
Preprint. Discussion started: 16 November 2022

Strasser, U., Bernhardt, M., Weber, M., Liston, G. E., and Mauser, W.: Is snow sublimation important in the alpine water balance?, The Cryosphere, 2, 53–66, https://doi.org/10.5194/tc-2-53-2008, 2008.

Vernay, M., Lafaysse, M., Monteiro, D., Hagenmuller, P., Nheili, R., Samacoïts, R., Verfaillie, D., and Morin, S.: The S2M meteorological and snow cover reanalysis over the French mountainous areas: description and evaluation (1958–2021), Earth Syst. Sci. Data, 14, 1707–1733, https://doi.org/10.5194/essd-14-1707-2022, 2022.

Vionnet, V., Brun, E., Morin, S., Boone, A., Faroux, S., Le Moigne, P., Martin, E., and Willemet, J.-M.: The detailed snowpack scheme Crocus and its implementation in SURFEX v7.2, Geosci. Model Dev., 5, 773–791, https://doi.org/10.5194/gmd-5-773-2012, 2012.

Westermann, S., Ingeman-Nielsen, T., Scheer, J., Aalstad, K., Aga, J., Chaudhary, N., Etzelmüller, B., Filhol, S., Kääb, A., Renette, C., Schmidt, L. S., Schuler, T. V., Zweigel, R. B., Martin, L., Morard, S., Ben-Asher, M., Angelopoulos, M., Boike, J., Groenke, B., Miesner, F., Nitzbon, J., Overduin, P., Stuenzi, S. M., and Langer, M.: The CryoGrid community model (version 1.0) – a multi-physics toolbox for climate-driven simulations in the terrestrial cryosphere, Cryosphere, https://doi.org/10.5194/gmd-2022-127, 2022.

Winstral, A., Elder, K., and Davis, R. E.: Spatial Snow Modeling of Wind-Redistributed Snow Using Terrain-Based Parameters, J. Hydrometeorol., 3, 524–538, https://doi.org/10.1175/1525-7541(2002)003<0524:SSMOWR>2.0.CO;2, 2002.

Wirz, V., Schirmer, M., Gruber, S., and Lehning, M.: Spatio-temporal measurements and analysis of snow depth in a rock face, The Cryosphere, 5, 893–905, https://doi.org/10.5194/tc-5-893-2011, 2011.

Woo, M. and Heron, R.: Occurrence of Ice Layers at the Base of High Arctic Snowpacks, Arct. Alp. Res., 13, 225, https://doi.org/10.2307/1551198, 1981.

Woo, M., Heron, R., and Marsh, P.: Basal Ice in High Arctic Snowpacks, Arct. Alp. Res., 14, 251, https://doi.org/10.2307/1551157, 1982.

Zevenbergen, L. W. and Thorne, C. R.: Quantitative analysis of land surface topography, Earth Surf. Process. Landf., 12, 47–56, https://doi.org/10.1002/esp.3290120107, 1987.